Evaluation of Domain Spacing Scaling Laws for Semicrystalline Diblock Copolymers

Konstadinos C. Douzinas and Robert E. Cohen*

Department of Chemical Engineering, Massachusetts Institute of Technology, 77 Massachusetts Avenue, Cambridge, Massachusetts 02139

Adel F. Halasa

The Goodyear Tire and Rubber Company, Research Division, 142 Goodyear Boulevard, Akron, Ohio 44305-0001

Received February 1, 1991; Revised Manuscript Received March 21, 1991

ABSTRACT: Diblock copolymers of (ethylene-*co*-butylene)–ethylethylene (EBEE) were used to evaluate scaling laws describing the molecular weight dependence of the lamellar domain spacing of semicrystalline block copolymer systems. Small-angle X-ray scattering was used to measure lamellar domain spacings for a series of EBEE samples. Experimental results were in good agreement with the predictions of the equilibrium theory of Whitmore and Noolandi.

Introduction

The molecular weight dependence of lamellar microdomain spacings of amorphous microphase-separated block copolymer systems has been extensively studied.[1-7] Existing theories use various approaches to arrive at a power law expression

$$D \propto Z_t^a \tag{1}$$

where Z_t is the total degree of polymerization of the amorphous diblock and a is an exponent less than unity, usually in the range of 0.6–0.8. Experimental verification of this power law has been attempted by using styrene–isoprene[8,9] and styrene–2-vinylpyridine[10] diblock copolymers. These studies have shown that a value of $^2/_3$ for the exponent accurately represents the domain spacing behavior in most cases over a wide range of molecular weights. This validates the use of Gaussian chain modeling for amorphous blocks in confined microdomains.

In the case of semicrystalline diblock copolymers, however, the theoretical description of the equilibrium state becomes more complicated since the possibility of crystallization of one of the blocks must be taken into account. An equilibrium theory has been proposed by Whitmore and Noolandi,[11] using a chain-folding model for the crystallizable block, a Gaussian chain model for the amorphous block, and localization of the chemical junction, which connects the two blocks in a narrow interface. The power law that describes the behavior of the lamellar long period is

$$D \propto Z_t Z_a^{-5/12} \tag{2}$$

where Z_t is the total degree of polymerization and Z_a is the degree of polymerization of the amorphous block. DiMarzio et al.[12] developed a similar power law with a different exponent for the amorphous block contribution:

$$D \propto Z_t Z_a^{-1/3} \tag{3}$$

These theories have not been critically tested yet. As has been shown for styrene–(ethylene-*co*-butylene) (SEB) copolymers,[13] the processing history used in sample preparation is critical in determining whether a kinetically locked or equilibrium morphology is achieved. Past studies of styrene–(ethylene oxide),[14-18] styrene–ϵ-caprolactone,[19,20] and butadiene–(ethylene oxide)[21] semicrystalline diblocks have not addressed this matter in detail. In this work we attempt to evaluate the scaling law using a model system of (ethylene-*co*-butylene)–ethylethylene (EBEE). EBEE is well suited to this purpose because it fulfills the requirements of the theory: EBEE has a very narrow molecular weight distribution, the crystallization behavior of the ethylene-*co*-butylene block is thoroughly understood,[22] and EBEE can be easily processed to give films with the necessary equilibrium morphology.

Experimental Section

EBEE diblock copolymer samples were prepared by catalytic hydrogenation of precursor diblocks of 1,4-polybutadiene–1,2-polybutadiene (4B2B), which were polymerized anionically. The 1,4-PB blocks contained 45% cis-1,4, 45% trans-1,4, and 10% vinyl repeat units. The 1,2-PB blocks were 99% atactic 1,2. Transmission electron microscopy was carried out on several of these precursor copolymers using staining procedures described earlier.[23] A typical result is shown in Figure 1. The catalytic hydrogenation procedure is described in detail elsewhere.[13,24] It is important to note that we have carefully verified that the hydrogenation of the 4B2B diblocks is complete and that there is no degradation, chain scission, or chain coupling of the 4B2B precursor molecules. The molecular weights of the 4B2B samples were measured by using GPC complemented by ^{1}H NMR; the corresponding molecular weights of EBEE were calculated by using the stoichiometry of the hydrogenation reaction. These molecular weights are listed in Table I. EBEE films were prepared by spin casting[25] from 5 wt % xylene solutions at 95 °C. The films were subsequently dried under vacuum. This processing history leads to microphase separation prior to crystallization, which gives the required equilibrium lamellar morphology. Variations in spin-casting temperature can lead to direct crystallization out of solution and kinetically locked spherulitic morphologies.[13]

SAXS measurements were performed at room temperature by using a Rigaku rotating Cu anode X-ray source (λ = 1.54 Å) with a Charles Supper double mirror focusing system and a Nicolet 2D area detector. The sample to detector distance was varied between 220 and 245 cm, and a helium-filled beam-line tube was used to reduce background scattering. Scattering measurements were performed by using three sample orientations with the X-ray beam parallel to the X, Y, and Z axes as shown in Figure 2. The raw scattered intensities were corrected for sample absorption, detector inhomogeneities, and background scattering.

Results

A sample set of 2D scattered intensity patterns is shown in Figure 3. The corresponding intensity ($I(Q)$) vs

0024-9297/91/2224-4457$02.50/0

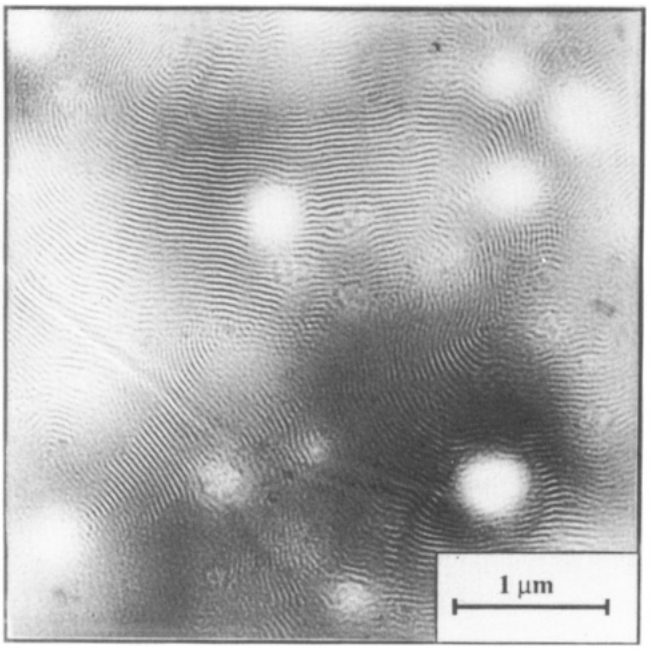

Figure 1. TEM micrograph of the 4B2B precursor for EBEE-144 (62/72).

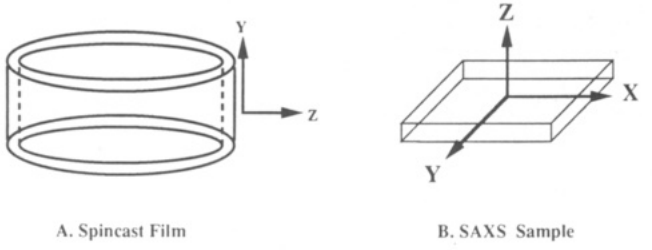

A. Spincast Film B. SAXS Sample

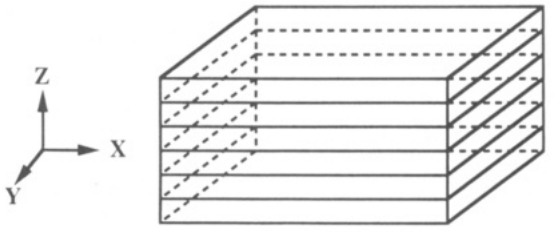

C. Proposed Lamellar Structure.

Figure 2. Sample and microstructure orientation for SAXS experiments.

Table I
Molecular Weight Characterization of EBEE

sample	$M_n \times 10^{-3}$ (GPC–NMR)	M_w/M_n (GPC)
EBEE-1	60/7	1.09
EBEE-2	36/6	1.03
EBEE-3	19/3	1.07
EBEE-136	82/76	1.20
EBEE-138	35/53	1.14
EBEE-140	81/35	1.11
EBEE-142	52/89	1.10
EBEE-144	62/72	1.11
EBEE-146	91/71	1.18
EBEE-148	124/63	1.12

scattering vector magnitude (Q) plot for irradiation parallel to the X axis is shown in Figure 4, where $Q = (4\pi/\lambda) \sin \theta$ and the scattering angle is 2θ. Arcs are observed in the 2D pattern when the samples are irradiated parallel to the

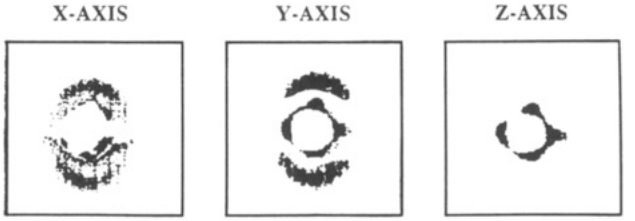

Figure 3. 2D SAXS patterns for EBEE-144 (62/72).

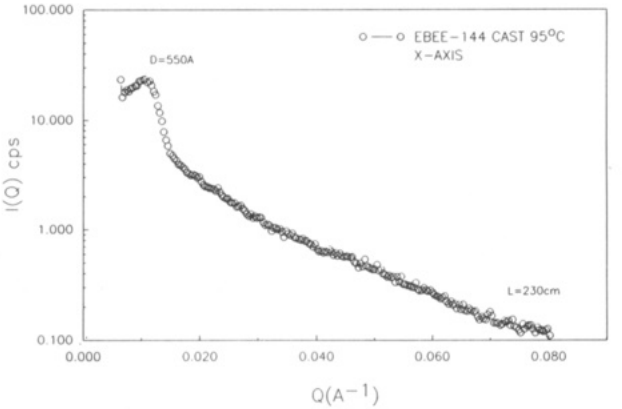

Figure 4. Average scattered intensity for EBEE-144 along the X axis.

Table II
Comparison of Experimental Lamellar Long Periods with Theoretical Predictions

				D, Å		
sample	$M_n \times 10^{-3}$	Z_t	Z_a	Noolandi	DiMarzio	measd
EBEE-1	60/7	1204	130	720	590	680
EBEE-2	36/6	759	111	480	390	520
EBEE-3	19/3	389	56	330	250	*a*
EBEE-136	82/76	2815	1352	630	640	650
EBEE-138	35/53	1574	944	410	400	460
EBEE-140	81/35	2074	629	640	600	680
EBEE-142	52/89	2519	1593	530	540	520
EBEE-144	62/72	2389	1278	550	550	550[b]
EBEE-146	91/71	2889	1259	670	670	650
EBEE-148	124/63	3352	1130	810	800	*c*

[a] Sample EBEE-3 was homogeneous and had virtually no crystallinity. [b] The D spacing of EBEE-144 was used as a convergence point for comparing the slopes of theoretically predicted and experimentally measured scaling laws. [c] The D spacing of sample EBEE-148 was too large to be measured with the existing SAXS setup.

X and Y axis, while there is no significant scattering when the samples are irradiated parallel to the Z axis. This information indicates that the lamellae are predominantly parallel to the XY plane, but their orientation is not perfect. The lamellar domain spacing, or long period D, is calculated from these data by using Bragg's diffraction law $D = 2\pi n/Q_p$, where Q_p is the magnitude of the scattering vector at the intensity peak position and n is the peak order. In all our samples we observed only primary peaks; i.e., $n = 1$. Values for the lamellar domain spacing of our samples are shown in Table II.

Discussion

Plots to examine the two scaling laws are shown in Figures 5 and 6. The lines appearing in these plots are not best fit lines based on linear regression but rather predictions of the scaling laws for the D spacing as explained in footnote *b* of Table II. Both theories seem to adequately predict the general trend of the data within experimental error. Although it is difficult to differentiate

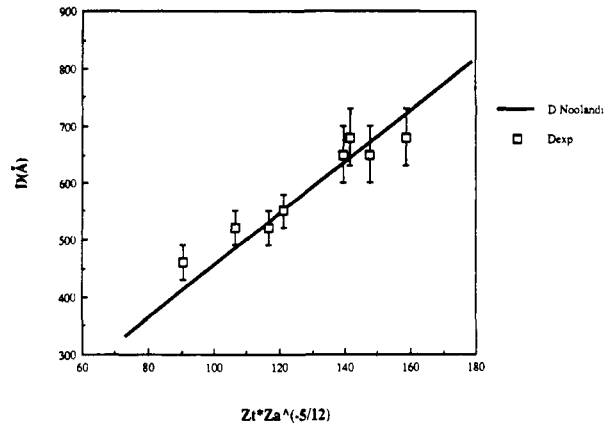

Figure 5. Noolandi scaling law.

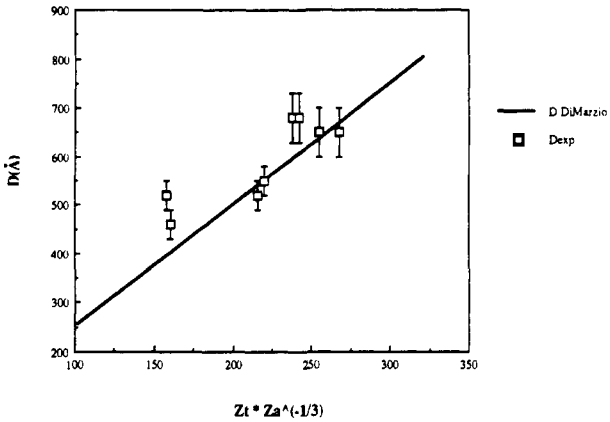

Figure 6. DiMarzio scaling law.

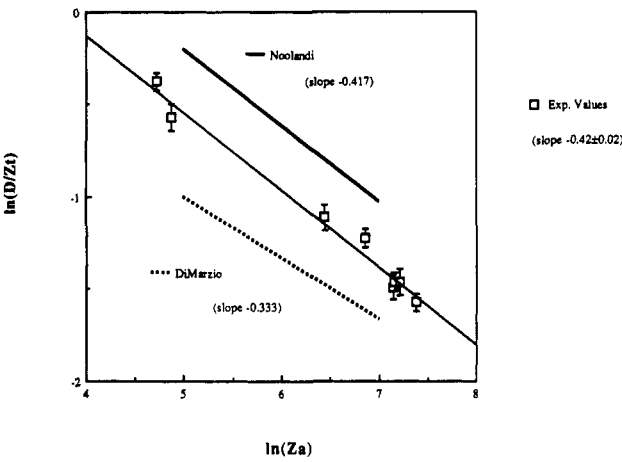

Figure 7. Comparison of Noolandi and DiMarzio scaling laws. (Theoretical lines are displayed for slope comparison only.)

between the two theoretical models, due to resolution limitations of SAXS measurements of D spacings, to test the validity of eqs 2 and 3, we have plotted $\ln (D/Z_t)$ versus $\ln Z_a$ in Figure 7. The theories predict straight lines with slopes of $-5/12$ (Noolandi) and $-1/3$ (DiMarzio). Such lines are shown in Figure 7 only for slope comparison, and their position on the vertical axis has been arbitrarily chosen to clearly illustrate the relationship between predicted and experimental slopes. The least-squares best fit to the experimental data for the EBEE samples gives a line with a slope of -0.42 ± 0.02, which, for practical purposes, is indistinguishable from $-5/12$. We conclude that Noolandi's theory achieves a slightly better prediction of the scaling behavior of the lamellar long period in semicrystalline diblock copolymers.

It is extremely interesting to note that some of the semicrystalline EBEE block copolymer samples with significantly different molecular weights display almost identical lamellar spacings, while their amorphous counterparts always exhibited larger spacings with increased molecular weight as predicted by eq 1. The different behavior of the semicrystalline diblocks can be understood by taking into account the degree of chain folding in the EB block.[11] The equilibrium degree of chain folding is affected by the transverse dimensions of the flexible amorphous chain. If the molecular weight of the crystalline block remains constant and the molecular weight of the amorphous block increases, the crystalline chain will have to fold more to accommodate the increase in the transverse dimensions of the amorphous chain. This increased amount of folding leads to a corresponding decrease in the thickness of the crystalline lamellae. It is therefore possible for increases in the thickness of the amorphous lamellae to be counterbalanced by decreases in the thickness of the crystalline lamellae; thus the lamellar long period may remain virtually unaffected despite the change in block molecular weights.

The actual orientation of the chain-folded molecules with respect to the lamellar microdomain structure is also of great interest. According to Noolandi's model, the chain axis of the EB blocks is assumed to be essentially normal to the plane of the lamellae. In other words, the EB chains are taken to be parallel to the Z axis. Experimental examination of this assumption is currently being carried out on EBEE samples using wide-angle X-ray diffraction pole figure analysis.

Acknowledgment. This research was supported by the Office of Naval Research, The Goodyear Tire and Rubber Co., and by the Bayer Professorship in Chemical Engineering at M.I.T.

References and Notes

(1) Meier, D. J. *Block and Graft Copolymers*; Burke, J. J., Weiss, V., Eds.; Syracuse University Press: Syracuse, NY, 1973.
(2) Meier, D. J. *Polym. Prepr. (Am. Chem. Soc., Div. Polym. Chem.)* **1974**, *15*, 171.
(3) Helfand, E. *Macromolecules* **1975**, *8*, 552.
(4) Helfand, E.; Wasserman, Z. R. *Macromolecules* **1976**, *9*, 879.
(5) Helfand, E.; Wasserman, Z. R. *Macromolecules* **1978**, *11*, 960.
(6) Leibler, L. *Macromolecules* **1980**, *13*, 1602.
(7) Hashimoto, T. *Macromolecules* **1982**, *15*, 1548.
(8) Hashimoto, T.; Shibayama, M.; Kawai, H. *Macromolecules* **1980**, *13*, 1237.
(9) Hadziioannou, G.; Skoulios, A. *Macromolecules* **1982**, *15*, 258.
(10) Matsushita, Y.; Mori, K.; Saguchi, R.; Nakao, Y.; Noda, I.; Nagasawa, M. *Macromolecules* **1990**, *23*, 4313.
(11) Whitmore, M. D.; Noolandi, J. *Macromolecules* **1988**, *21*, 1482.
(12) DiMarzio, E. A.; Guttman, C. M.; Hoffman, J. D. *Macromolecules* **1980**, *13*, 1194.
(13) Cohen, R. E.; Cheng, P.-L.; Douzinas, K.; Kofinas, P.; Berney, C. V. *Macromolecules* **1990**, *23*, 324.
(14) Lotz, B.; Kovacs, A. J. *Kolloid Z. Z. Polym.* **1966**, *209*, 97.
(15) Lotz, B.; Kovacs, A. J.; Bassett, G. A.; Keller, A. *Kolloid Z. Z. Polym.* **1966**, *209*, 115.
(16) Gervais, M.; Gallot, B. *Makromol. Chem.* **1973**, *171*, 157.
(17) Gervais, M.; Gallot, B. *Makromol. Chem.* **1973**, *174*, 193.
(18) Gervais, M.; Gallot, B. *Makromol. Chem.* **1977**, *178*, 2071.
(19) Herman, J.-J.; Jerome, R.; Teyssie, P.; Gervais, M.; Gallot, B. *Makromol. Chem.* **1978**, *179*, 1111.
(20) Gervais, M.; Gallot, B. *Makromol. Chem.* **1981**, *182*, 997.
(21) Gervais, M.; Gallot, B. *Makromol. Chem.* **1978**, *178*, 1577.
(22) Howard, P. R.; Crist, B. *J. Polym. Sci., Part B: Polym. Phys.* **1989**, *27*, 2269.
(23) Cohen, R. E.; Wilfong, D. E. *Macromolecules* **1982**, *15*, 370.
(24) Halasa, A. F. U.S. Patent 3 872 072.
(25) Bates, F. S.; Cohen, R. E.; Argon, A. S. *Macromolecules* **1983**, *16*, 1108.